Turkish Journal of Electrical Engineering and Computer Sciences

Volume 32 | Number 2 Article 2

3-14-2024

Intelligent protection scheme using combined Stockwell-Transform and deep learning-based fault diagnosis for the active distribution system

LATHA MAHESWARI KANDASAMY
klm.eee@psgtech.ac.in

KANAKARAJ JAGANATHAN
jkr.eee@psgtech.ac.in

Turkish Journal of Electrical Engineering & Computer Sciences

http://journals.tubitak.gov.tr/elektrik/

Research Article

Turk J Elec Eng & Comp Sci
(2024) 32: 234 – 250

doi:10.55730/1300-0632.4066

Intelligent protection scheme using combined Stockwell-Transform and deep learning-based fault diagnosis for the active distribution system

Latha Maheswari KANDASAMY*, **Kanakaraj JAGANATHAN**
Department of Electrical and Electronics Engineering, PSG College of Technology, Peelamedu, Coimbatore, Tamilnadu, India

Received: 01.03.2023 • **Accepted/Published Online:** 20.08.2023 • **Final Version:** 14.03.2024

Abstract: This study aims to perform fast fault diagnosis and intelligent protection in an active distribution network (ADN) with high renewable energy penetration. Several time-domain simulations are carried out in EMTP-RV to extract time-synchronized current and voltage data. The Stockwell transform (ST) was used in MATLAB/SIMULINK to preprocess these input datasets to train the adaptive fault diagnosis deep convolutional neural network (AFDDCNN) for fault location identification, fault type identification, and fault phase-detection for different penetration levels. Based on the AFDDCNN output, the intelligent protection scheme (IDOCPS) generates the signal for isolating a faulty section of the ADN. An intelligent fault diagnosis scheme that combines ST and deep learning methods aids the artificial intelligence-based protection scheme in isolating the faulty section. This study uses the PyTorch framework to build both the AFDDCNN and IDOCPS. The proposed protection technique classifies and isolates faults and coordinates protection with minimum operating time in the IEEE 13-bus ADN. It consistently gives high accuracy for fault diagnosis and minimum operating time for the IDOCPS even when the network's topology is modified to the IEEE 34-bus ADN. The experimental results indicate that the proposed model is more accurate and provides faster fault diagnosis and isolation than state-of-the-art methods.

Key words: Distributed energy resources, Stockwell transform, deep convolutional neural network, phasor measurement units, distributed generation, multilayer perceptron, multiobjective firefly algorithm

1. Introduction

Distributed energy resources (DERs) are connected to distribution systems to meet rising energy demands, optimal operation requirements, and the need to reduce greenhouse gas emissions. Protection and control of distribution systems (DSs) have become difficult due to the integration of time-varying low inertia inverter interfaced distributed generations (IIDG) [1, 2]. The fault current level in the DS changes according to the penetration level, type, and location of the distributed generation (DG). While designing a protection scheme, neglecting the above-mentioned challenges causes relay coordination loss, protection blinding, unintentional islanding, and sympathetic tripping [2]. The phasor measurement units (PMUs) allow real-time dynamic monitoring of the DS, and fault zone identification is simpler with correctly allocated PMUs. The authors of [1] utilize μPMU data and a stacked autoencoder (SAE) for fault location in the DS, but they neglected the fault classification and the effect of high impedance fault (HIF) on the algorithm. The study presented in [2] proposed intelligent microgrid fault diagnosis using a deep learning model. Even though various operating conditions

*Correspondence: klm.eee@psgtech.ac.in

were considered, the increased computation time for Fourier-based continuous wavelet transform (FTCWT), complexity in locating faults, and disregarded protection coordination aspect is their major drawback. The authors of [3] proposed time-synchronized protection for fault diagnosis of a microgrid by extracting statistical features from the PMU data for the k-nearest neighbor (kNN) module. In [4], the authors proposed an intelligent protection scheme based on the TT transformation and deep belief network, while [5] utilizes adaptive convolution neural network (ACNN) for fault location in DS. The authors of [6] proposed a hybrid classifier for fault location in active distribution networks (ADN). Further, these researchers [4–7] focused more on fault identification and location, but the protection aspect of the DS and time complexity analysis were not considered. The authors of [8] recommended applying an enhanced extreme learning machine (ELM) based on the discrete orthonormal ST (DOST) for intelligent fault diagnosis. Even though various fault scenarios were created to depict the efficacy of the proposed method, HIF, scalability for the larger DS, suggested method performance comparison and its computing time were neglected. In [9], DOST-support vector machine (SVM)-based fault diagnosis for transmission systems was presented utilizing the synchronized current measurements from remote terminal units (RTUs). However, these methods are ineffective for short distribution lines, DS with varying DER penetration, and fault resistance. The fuzzy sets for fault diagnosis and protection coordination with optimization algorithms were reported in [10–14]. However, multiple optimal settings and miscoordination were observed due to difficulty in establishing global minimums using fuzzy membership functions. In [15], the authors proposed utilizing the grey wolf optimizer algorithm to determine the optimal overcurrent relay (OCR) and distance relay settings for the transmission system, while [16] utilized the rate of change of phasor voltage for coordination in a medium voltage DS. However, the methodology suggested in [15] and [16] is ineffective for a low-voltage ADN. The study presented in [17] utilized the firefly algorithm (FA) for fault detection and protection coordination in a DS; however, the heuristic algorithm failed to find the global optimum and converge to practically effective solutions due to the lack of a universally applicable method. In addition to monitoring the power grid with PMUs, the difficulty of optimizing PMU deployment has attracted considerable interest due to the high cost of PMU installation [18]. In [19], an algorithm was proposed to identify optimal deployment for measurement devices (PMUs and smart meters) considering variable DER integration. Most previously reported DS protection schemes are limited to detecting the fault without identifying the faulty line segment or examining whether the other healthy lines remain unaffected without tripping. Intelligent protection requires an adaptive fault diagnosis approach for effective fault phase identification and isolation in the DS. The centralized intelligent decision-making mechanism based on PMUs employed in the present work addresses this issue by utilizing a relay that would only trip the faulty line between two buses.

This study utilizes a DOST for preprocessing the input dataset that retains all the critical data for a novel artificial intelligence (AI)-based classification algorithm. The proposed adaptive fault diagnosis effectively performs fault detection, classification, and location tasks utilizing current and voltage data from the time-synchronized PMUs placed at the appropriate location on the ADN. Furthermore, the developed intelligent protection scheme utilizes the adaptive fault diagnosis output to identify and isolate the faulty section with minimum operating time (OT) under various ADN operating conditions. The significant contributions of the proposed work can be summarized as follows: i) The adaptive fault diagnosis unit developed using an adaptive fault diagnosis deep convolutional neural network (AFDDCNN) performs the task of exact fault phase and location identification for various operating modes of the ADN. ii) An intelligent protection algorithm that utilizes the multiobjective firefly algorithm (MOFFA), and multi-layer perceptron (MLP) is proposed for the

protection and coordination of directional OCR (DOCR). iii) Supervised learning of MLP is used to select the best optimal protection strategy with an appropriate setting for the different operating scenarios. iv) The effectiveness of the proposed algorithm is assessed for modified IEEE 13-bus and IEEE 34-bus ADNs. v) Based on the response time the superiority of the proposed algorithm is compared with other protection techniques reported in the literature. The paper's organization is as follows: Section 2 introduces the investigated test ADN utilized in the proposed work; Section 3 describes the proposed intelligent fault diagnostic unit (AFDDCNN) for fault identification, classification, and isolation along with the implementation and dataset preparation from the test system; Section 4 describes the proposed intelligent protection scheme (IDOCPS) for primary protection, backup protection and protection coordination in the test ADN; Section 5 verifies the effectiveness of the proposed model and the adaptability of the algorithm to larger ADN; and Section 6 gives a detailed performance analysis of the proposed method with other methods listed in the literature; Finally, Section 7 concludes the paper with the limitations of the proposed methodology, and directions for future work on ADNs protected using the proposed intelligent protection scheme.

2. Investigated distribution system

The modified IEEE 13-bus and IEEE 34-bus ADNs [20, 21] examined for the proposed protection method and simulated in EMTP 4.2.85, 2019®, are shown in Figures 1a and 1b. The IEEE 13-bus ADN includes two DFIG wind generators (DG1 and DG3) of 150 kW connected at nodes 671 and 634, one wind farm with four DFIG wind generators (DG3) of 1 MW capacity connected to node 675, and one PV unit (DG4) of 750 kW connected at node 652. High DG penetration is achieved by modifying the IEEE 34-bus ADN to include IIDG at nodes 820, 822, and 844, asynchronous wind generators at nodes 848 and 890 and synchronous generators at nodes 840 and 864 [2]. Sensitivity analysis was performed to determine the optimal number of PMUs to minimize the cost of utilities and the technical limitations associated with communication aspects [18]. PMUs at generation sources provide current and voltage measurements for the fault location identification algorithm. As shown in Figure 1, this results in 4 PMUs for IEEE 13-bus ADN and 9 PMUs for IEEE 34-bus ADN nearer to DER throughout the network for constant monitoring. The dataset preparation using S-transform was performed in the MATLAB/SIMULINK environment on a computer with a 32 GB RAM Intel Core i7 3.20 GHz processor under various operating conditions as described in [2]. Two cycles of current and voltage waveforms obtained from the PMU location for each fault/nonfault scenario are converted into a time-frequency pattern using the DOST. The AFDDCNN is trained on these patterns as input to diagnose the fault in the ADN.

3. Proposed adaptive fault diagnostic methodology

3.1. Implementation and dataset preparation

ST utilizes progressive resolution with absolutely referenced phase and frequency information to generate a time-frequency pattern for the given signal [22]. Eq. (1) computes the continuous ST for a given input signal h(t).

$$S(\tau, f) = \frac{|f|}{\sqrt{2\pi}} \int_{-\infty}^{\infty} h(t) e^{\frac{-(\tau-t)^2 f^2}{2}} e^{-i2\pi f t} dt \tag{1}$$

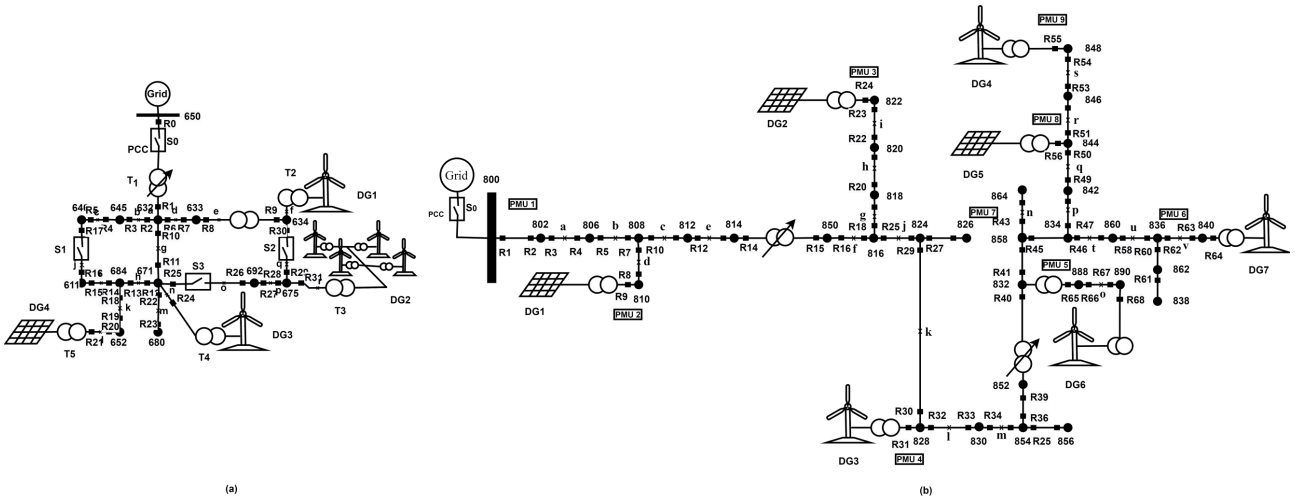

Figure 1. (a) Investigated IEEE 13-bus ADN model with DG; (b) investigated IEEE 34-bus ADN model with DG.

Here, τ, f, and $\frac{1}{\sqrt{2}}\int_{-\infty}^{\infty} e^{\frac{-(\tau-t)^2 f^2}{2}} dt = \frac{\sqrt{2\pi}}{|f|}$ are the time, frequency, and Gaussian window functions, respectively. This paper uses DOST, which localizes the spectrum while retaining beneficial ST phase features and reducing redundancy in the time-frequency representation [23]. Eq. (2) provides an effective representation of DOST.

$$S_{[v,\beta,\tau]}[kT] = \frac{ie^{-i\pi\tau}}{\sqrt{\beta}} \frac{\left\{ e^{-i2\pi\left(\frac{k}{N}-\frac{\tau}{\beta}\right)\left(v-\frac{\beta}{2}-\frac{1}{2}\right)} - e^{-i2\pi\left(\frac{k}{N}-\frac{\tau}{\beta}\right)\left(v+\frac{\beta}{2}-\frac{1}{2}\right)} \right\}}{2Sin\left(\pi\left(\frac{k}{N}-\frac{\tau}{\beta}\right)\right)} \tag{2}$$

Here, v is a frequency variable representing the center of a frequency band, β indicates the frequency resolution, and τ is a time variable that indicates the time localization. The following rules are applied to sample the time-frequency space to ensure orthogonality: Rule 1: $\tau = 0, 1, \ldots, \beta - 1$; Rule 2: v and β must be selected such that each Fourier frequency sample is used once and only once [22, 24]. Using octave sampling with variable p representing the octave number $p = 0, 1, 2, \ldots, log^2 N - 1$ the parameters (v, β, τ) change for $p > 1$, $p = 2, ..., \log^2 N - 1$, $\beta = 2(p-1)$, $\tau = 0, 1, \ldots, 2(p-1) - 1$, $v = 2(p-1) + 2(p-2)$, which modifies Eq. (2). The current and voltage waveforms obtained when a line–ground (LG) fault occurs at distribution line 3 (DL3) of the test system are shown in Figure 2a. The time-frequency pattern obtained by applying DOST for the faulted phase current in the test system is shown in Figure 2b. Furthermore, the time-frequency patterns obtained for all the phase voltage and current for a particular scenario act as labeled input datasets to the AFDDCNN. Similarly, the test system can obtain the voltage, current, and time-frequency patterns by simulating various operating conditions as mentioned in [2]. The dataset obtained with 50,000 fault cases and 1,158 no-fault cases from EMTP-RV are used for training the AFDDCNN model. The fault cases

include the labeled datasets of AG, BG, CG, AB, AC, BC, ABG, ACG, BCG, ABC, and ABCG at different operating scenarios like DG1 out, DG2 out, DG3 out, DG4 out, DG1 and DG2 out, DG2 and DG3 out, DG1 and DG3 out, DGP-140, DGP-120, DGP-100, DGP-75, and DGP-40. On the other hand, the no-fault cases include labeled datasets under normal operating conditions with different operating scenarios. Due to the rarity of faults during normal operation, the resulting current and voltage signals present an unbalanced dataset for classification. Therefore, the dropout regularization of the AFDDCNN model tackles overfitting issues that arise during training if the classifier is trained using an imbalanced dataset.

The architecture of the adaptive fault diagnostic deep convolutional neural network (AFDDCNN) employed for fault diagnosis is shown in Figure 3 [25]. It has an input layer, five convolutional layers with dropout regularization, three max-pooling layers, three fully connected layers, and an output layer. The vectorized activation of a layer in the AFDDCNN is defined in Eq. (3).

$$A^{[L]} = g^{[L]}(W^{[L]} * A^{[L-1]} + b^{[L]}) \tag{3}$$

Here, $W^{[L]}$ denotes a weight vector of the layer L, $b^{[L]}$ denotes a bias for layer L, "$*$" indicates the convolution operation, and $g^{[L]}$ is an activation function for layer L. The hyperparameters for the proposed AFDDCNN are determined based on Bayesian optimization and are listed in Figure 3. This involves finding the optimal set of hyperparameters such as learning rate, batch size, number of layers, filters, filter sizes, and dropout rate that yield the best performance for the fault diagnosis problem. The model adjusts its weights and biases to minimize the gap between projected and actual outputs using the training set (60%), while Bayesian optimization [26] utilizes the validation set (20%) to tune hyperparameters, and the test set (20%) evaluates the trained model's performance. By evaluating the model on the test dataset obtained using stratified sampling, model performance is estimated and advanced with intelligent decisions [27]. The optimized hyperparameter for training the proposed model utilizes a mini-batch size of 128 (2^7) with a learning rate of 0.0001 for 250 epochs.

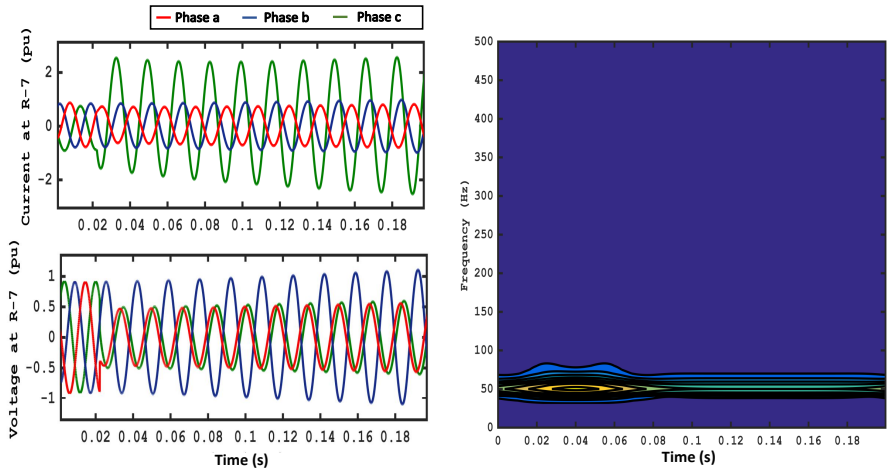

Figure 2. (a) Current and voltage waveforms for LG fault in DL3 at t = 0.0222 s ($\theta = 130^\circ$, Rf = 0.01 Ω, FL = 10%, LVAR = 50%, DGP =100%); (b) DOST of faulted phase current.

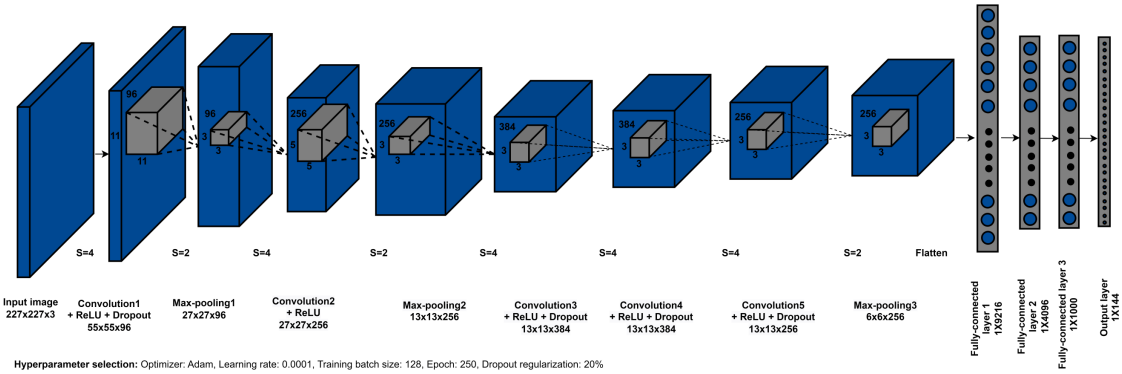

Figure 3. AFDDCNN architecture used for the proposed fault diagnosis

3.2. Fault detection and classification unit

The various steps in designing the proposed adaptive fault diagnosis framework are described in Figure 4. First, the AFDDCNN1 trained using the labeled dataset determines whether the fault is a low-impedance fault (LIF) or HIF. It consists of two convolution layers and a fully connected layer with two output neurons representing whether the fault is HIF/LIF. Next, the fault detection/classification unit (AFDDCNN2) helps with exact fault phase identification and classification. The fault detection and identification unit receives a time-frequency representation of the current and voltage dataset from the PMU as input to the AFDDCNN2, as shown in Figure 2. The proposed AFDDCNN2 architecture, as shown in Figure 3, utilizes five convolutional layers to extract hidden feature maps from the given data. The output feature is reduced by dropout regularization performed at the convolutional layer, preventing overfitting of the model.

Furthermore, the three maximum pooling layers described by Eq. (4) downsample the output features and eliminate redundant information. In addition, a rectified linear unit (ReLU) described by Eq. (5) is utilized as an activation function to get faster convergence and reduce the output feature. Eq. (6) represents the categorical cross-entropy loss function used for the classification task in the fault diagnosis unit.

$$a_j^{(l+1)} = Pool\left(a_1^{(l)}, \ \ldots, \ a_i^{(l)}, \ldots, a_n^{(l)}\right), \ i \in R_j^{(l)} \tag{4}$$

$$g(z) = max(0, z) = \begin{cases} z\_i & \text{if } z\_i \geq 0 \\ 0 & \text{if } z\_i < 0 \end{cases} \tag{5}$$

$$L(\widehat{y}, y) = \frac{1}{m}\sum_{i=1}^{m}\frac{(\widehat{y_i} - y_i)^2}{2} = -\frac{1}{m}\sum_{i=1}^{m}\sum_{j=1}^{n}((y_{ij} * log(\widehat{y_{ij}}) + (1 - y_{ij})log(1 - \widehat{y_{ij}})) \tag{6}$$

Here, $z = w * x + b$, y_{ij} is the actual distribution label and $\widehat{y_{ij}}$ is the predicted output distribution label from the AFDDCNN model. Finally, using convolution and pooling processes, three fully connected layers judge the features once they are extracted and downsampled. In the last fully connected layer, 144 neurons correspond to 132 faults and 12 no-fault cases. Furthermore, the softmax normalization expressed by Eq. (7) at the output layer determines credible fault types based on the probability of a multiclass fault classification problem.

$$F\left(X_i\right) = \frac{exp(X_i)}{\sum_j^k exp(X_j)} i = 0, 1, 2, \ldots, k \tag{7}$$

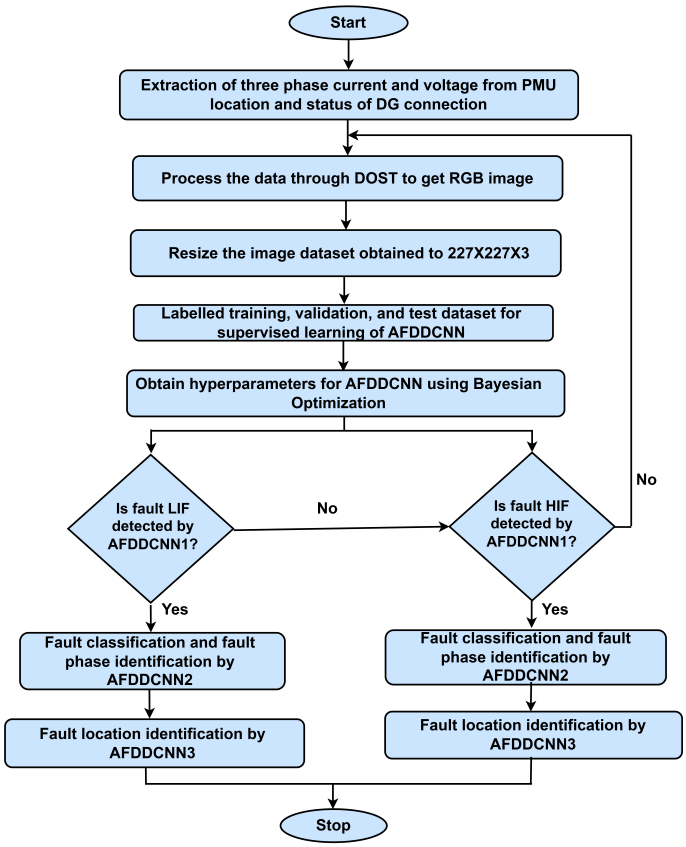

Figure 4. AFDDCNN architecture used for the proposed fault diagnosis

3.3. Fault location identification unit

The fault location identification unit (AFDDCNN3) recognizes the precise ADN's fault location for different instances and identifies the correct defective line. The AFDDCNN3 utilizes regression to identify the fault location in the distributed line section from the pretrained model. The root mean squared logarithmic error (RMSLE) loss function described in Eq. (8) is the objective function (OF) to be optimized throughout the learning process of the regression AFDDCNN3 to minimize errors in the model.

$$L(\widehat{F_L}, F_L) = \sqrt{\frac{1}{m}\sum_{i=1}^{m}\left(log(\widehat{F_L}) - log(F_L)\right)^2} \tag{8}$$

Here, $\widehat{F_L}$ and F_L are the predicted and exact fault locations, respectively. As the time-synchronized DL current and voltage data include nondiscriminating data at different fault locations; AFDDCNN3 has an additional convolutional layer to locate faults accurately. The output regression layer indicates the faulted DL section (DL1, DL2, DL3, DL4, DL5, DL6, DL7, DL8, DL9, and DL10) with the exact fault location. The intelligent protection unit utilizes this information to remove the faulty section without disrupting the other healthy DLs.

4. Proposed intelligent directional overcurrent protection unit

The ADN's high DG penetration and dynamic load condition necessitate an intelligent relay algorithm with multiple protective settings. Eq. (9) employs the fault current ratio obtained from current measurements to evaluate the OT for the conventional DOCR utilized in the DS [16, 28].

$$Operating\ time\ t = \frac{(\lambda * TMS)}{(\frac{I_F}{PS}^{\gamma} - 1)} + L \tag{9}$$

Here, λ, γ , and L are the characteristic relay constants, and CS is the curve setting for the DOCR. In Eq. (9), I_F , PS, TMS indicates the fault current, plug setting, and time multiplier setting of the DOCR. One of the challenges in ADN protection coordination is the need to consider multiple objectives, such as minimizing protective device OT while maintaining system stability and minimizing power losses. With a directional feature, the novel IDOCPS built using MLP and MOFFA employed in this paper enables different protective settings for varying operating conditions. The architecture of an MLP with a hidden layer, input layer, and output layers that utilize the Levenberg–Marquardt backpropagation learning method is shown in Figure 5a [29]. The various relay settings for different operating modes are provided for the offline training of the MLP to select the appropriate coordination setting for the given configuration.

The backpropagation algorithm enables the network to update its weights and biases to minimize errors between the predicted and actual outputs during training. This iterative process continues until the network converges to a state where the error is minimized. MOFFA is a variant of the FA used to solve optimization problems with multiple objectives [30]. MOFFA is a bioinspired swarm intelligent optimization technique to solve the proposed scheme's multiobjective nonlinear coordination problem [30, 31]. In MOFFA, the basic FA is modified to handle multiple OFs using Pareto dominance to determine the best solutions. MOFFA uses a population of fireflies, each representing a candidate solution to the optimization problem. These fireflies move towards brighter and better solutions, and the movement of the fireflies is based on the attractiveness between them, which is determined by their relative fitness. These nondominated solutions form the Pareto front, representing the optimal trade-offs between the different objectives. The multi-OF with n objectives is given by Eq. (10) and is subjected to an inequality constraint $g_i \leq 0;\ i = 1, 2, \ldots, j$ and equality constraints $h_i = 0;\ i = 1, 2, \ldots, k$.

$$Min\ f(x) = [f_1\ (x), f_2\ (x), \ldots, f_n\ (x)]^T \tag{10}$$

The structure of individual fireflies modified to represent the proposed intelligent directional overcurrent protection scheme (IDOCPS) is depicted in Figure 5b. MLP can learn from historical data and predict optimal coordination settings, while MOFFA can search for optimal protection settings (DOCR) in the wide operating conditions of the ADN [32]. MLP is used to formulate the problem of optimal OCR coordination. After formulating the problem, the TMS and $N_{IDOCPSi}$ of OCRs are determined using MOFFA. These values are then utilized as the starting decision in MLP, which results in the global optimal solution. The parameters and

stopping criteria for determining the MOFFA and MLP structure are represented in Figure 5c. An overview of the proposed IDOCPS algorithm is shown in Figure 5d. The IDOCPS utilizes the data obtained from the short circuit analysis of the ADN under various operating conditions [21, 23], the connection status of DG, primary and backup protection settings of the upstream and downstream relay, and the output of the AFDDCNN. In the IDOCPS, fireflies are chosen randomly, along with the operating constraint of protection coordination of the DOCR. Each firefly determines the optimal relay setting for that operating mode. The firefly with a minimum OF value is chosen as the best firefly, and the new protection settings are updated. Finally, the pretrained MLP determines the optimal relay setting to minimize the OT for the particular operating mode and sends the trip signal accordingly. Eq. (11) describes the main OF for optimizing the OT of the IDOCPS under different operating conditions. Eqs. (12) and (13) indicate the fault current and $N_{IDOCPSi}$ computation by the algorithm for the intelligent protection of the ADN. Eq. (11) is solved to get the minimum OT subjected to the relay characteristic constraint of Eq. (14) and the coordination constraint of Eq. (15). The difference between the backup relay ($t_{BRIDOCPSkl}$) and primary relay ($t_{PRIDOCPSkl}$) OTs must be optimized so that the coordination time interval (CTI) is minimal [13, 14].

$$Minimize \sum_{i=1}^{m} Operating\ time\ t_{IDOCPSi} = \frac{(\lambda_i * TMS_i)}{(N_{IDOCPSi}^{\gamma_i} - 1)} + L \ = \ \frac{1}{m} \sum_{i=1}^{m} \frac{(\widehat{y_i} - y_i)^2}{2} \tag{11}$$

$$N_{IDOCPSi} = \frac{(I_{ni} - \ I_{ni-1})}{I_{Pickup}} \tag{12}$$

$$I_{ni} = \sum_{i=1}^{m} (DG_{iStatus} \times \ I_{DGi} + \ I_{LFAnodei}) \tag{13}$$

$$I_{load}^{max} \leq N_{IDOCPSi} \leq \ I_{fault}^{min} \tag{14}$$

$$Coordination\ Time\ Interval\ (CTI) \leq t_{BRIDOCPSkl} - \ t_{PRIDOCPSkl} \tag{15}$$

Here, I_{ni} is the postfault current, $DG_{iStatus}$ is the status of the DG connection, I_{DGi} is the current contributed by the DG, $I_{LFAnodei}$ is current without DG connection, I_{Pickup} is the pickup current, k is the configuration index, l is the fault location and I_{ni-1} is the prefault current at the ith node of an ADN. The regression-based IDOCPS adopts TMS and N$_{IDOCPS}$ with DG uncertainty and penetration to accurately predict intelligent protection settings for each operating scenario. Based on the OT computed by Eq. (11), the IDOCPS generates the trip signal to isolate the appropriate section of the ADN without affecting the healthy phase of the ADN. When the primary relay fails to operate due to loss of communication, the backup relay acts after the time delay and isolates the faulty section.

5. Simulation results and discussion

The competence of the fault detection/classification, fault location identification, and intelligent protection units was evaluated based on investigations performed under various operating conditions [2]. The classifier accuracy, dependability, security, recall, and F1-score for performance evaluation of the developed AFDDCNN model were then calculated using the metrics indicated in Table 1 [2, 7, 21].

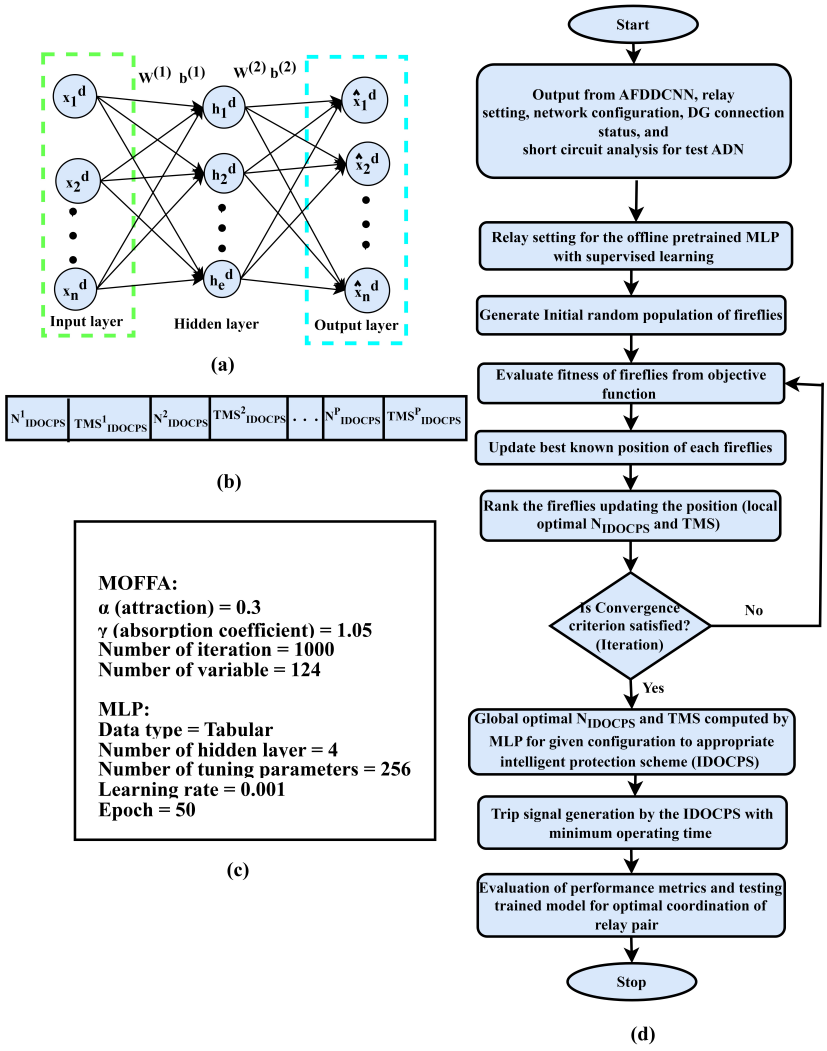

Figure 5. (a) Architecture of the MLP. (b) Structure of individual firefly in proposed hybrid MLP-MOFFA scheme (c) Parameter for determining the structure of MOFFA and MLP (d) Flowchart for the intelligent directional overcurrent protection scheme (IDOCPS).

Table 1. Formulae for evaluation of performance metrics for the proposed AFDDCNN [2, 7, 21].

S. no.	Performance metric	Formulae
1	Accuracy	$(Ncf + Ncn)/(Ncf + Ncn + Nwf + Nwn)$
2	Dependability	$Ncf/(Ncf + Nwn)$
3	Security	$Ncn/(Nwf + Ncn)$
4	Recall	$Ncf/(Ncf + Nwf)$
5	F1-score	$Ncf/(Ncf + 1/2(Nwf + Nwn))$

N_{cf} - Number of correct fault conditions, N_{cn} - number of correct normal conditions, N_{wf} - number of wrong fault conditions, N_{wn} - number of wrong normal conditions

5.1. Performance evaluation of the proposed fault diagnosis technique for different fault scenarios

The proposed method's effectiveness for detecting fault /no-fault scenarios using the ADN's fault detection unit (AFDDCNN1) is represented in Figure 6a. The suggested AFDDCNN1's average accuracy, dependability, security, F1 score, and recall value for HIF at 50% DG penetration in the ADN is 99.76%, 99.25%, 99.19%, 99.37% and 99.58%, respectively. The effectiveness of the proposed method for each fault type by fault classification unit (AFDDCNN2) in the ADN is represented in Figure 6b. The accuracy, dependability, security, F1 score and recall value for the AFDDCNN2 for 75% load variation in the ADN is 99.83%, 99.21%, 99.03%, 99.52%, and 99.47%, respectively. Hence, the overall accuracy of AFDDCNN1, AFDDCNN2, and AFDDCNN3 is 99.74%, 99.69%, and 99.58%, respectively. The error in locating precise faults in the DL is compromised when fault resistance is increased, which is demonstrated by 6c. It can be observed that the percentage error in locating fault ranges from 0.6% to 2% for fault resistance of 1000 Ω. The iterative prediction curve that represents the development of both training and validation losses across the epochs for an AFDDCNN are shown in Figure 6d; it was found that the prediction error rate was almost minimal when the number of epochs approached approximately250. Table 2 presents the training and testing accuracy of the proposed fault detection, classification and location unit and its comparison with the methodology suggested in [2]. It can be inferred from Table 2 that the proposed approach does not overfit for fault diagnosis since the accuracy is same across the two datasets. While a small drop in accuracy is to be anticipated between the training and test datasets, it is nevertheless evident that the method does not overfit for fault diagnosis.

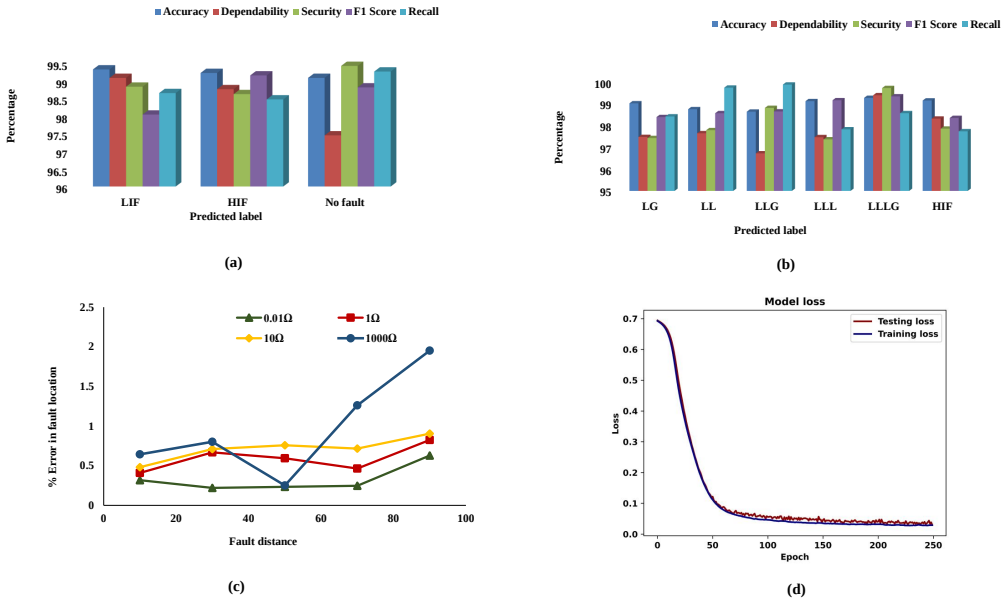

Figure 6. Performance analysis using statistical indices for (a) the proposed fault classification unit (AFDDCNN2), (b) the proposed fault detection unit (AFDDCNN1), (c) error in computing fault location by the proposed fault location unit (AFDDCNN3), and (d) loss vs epoch curve for the proposed AFDDCNN.

Table 2. Calculated fault detection, classification, and location units accuracy of the proposed AFDDCNN for the test ADN and comparison with results obtained for intelligent fault diagnosis in [2].

Fault type	Fault detection accuracy				Fault classification accuracy				Fault Location accuracy			
	Proposed AFDDCNN1		DCNN[2]	LSTM[2]	Proposed AFDDCNN2		DCNN[2]	LSTM[2]	Proposed AFDDCNN3		DCNN[2]	LSTM[2]
	Training	Testing	Testing	Testing	Training	Testing	Testing	Testing	Training	Testing	Testing	Testing
LG	99.73	99.65	98.19	99.61	99.83	99.58	97.73	98.61	99.78	99.52	98.02	98.87
LL	99.85	99.78	98.93	98.51	99.93	99.84	97.87	98.76	99.86	99.67	98.17	98.29
LLG	99.88	99.63	98.64	99.08	99.69	99.56	98.06	99.53	99.64	99.38	98.39	98.92
LLL	99.96	99.32	98.07	99.92	99.78	99.49	98.06	98.91	99.72	99.65	99.21	99.14
LLLG	99.91	99.59	98.79	98.3	99.85	99.67	98.22	98.03	99.57	99.48	98.83	98.27
HIF	99.87	99.76	98.16	99.12	99.74	99.31	96.88	97.79	99.69	98.97	98.62	97.36

DCNN - Deep convolutional neural network[2], LSTM - Long short-term memory[2].

5.2. Optimization results of the proposed intelligent protection technique

Table 3 indicates the variation of TSM_{PR1}, TSM_{BR1}, N_{PR1}, N_{BR1}, t_{PR1kl}, t_{BR1kl} of the IDOCPS for primary and backup protection for each fault node (a-r) in a grid-connected IEEE 13-bus test system with 75% DG penetration. The variables (TMS, N_{IDOCPS}) were initialized using the values acquired after running MOFFA for 1000 iterations, and the final values were determined using the MLP by determining the optimum OF with the lowest OT from Eq. (11). The CTI and maximum/minimum OT parameters obtained by the proposed scheme meet all OT criteria. Based on the proposed scheme, the backup protection relay for primary relay R24 is R25, with OTs equal to 0.3976 s for R24 and 0.7142 s for R25, resulting in a CTI of 0.3166 s for a fault at n that experienced miscoordination when using the conventional protection scheme. Relay R25 in the proposed strategy has a forward characteristic devoted to a fault at o and a reverse characteristic dedicated to a fault at m. Table 3 illustrates that both operating modes' average primary and backup protection OTs are 0.3359 s and 0.5893 s for the test IEEE 13-bus ADN in grid-connected mode with 75% DG penetration. Hence, the average OT of the IDOCPS for the modified IEEE 13-bus ADN is 0.4626 s for the grid-connected ADN. Similarly, the primary and secondary protection settings were obtained for the islanded mode of operation of the ADN. Table 4 indicates the variation of TSM_{PRI}, TSM_{BRI}, N_{PRI}, N_{BRI}, t_{PRIkl}, t_{BRIkl} of the IDOCPS for primary and backup protection of the grid-connected IEEE 34-bus test system with 40% DG penetration. It is observed from Table 4 that relay R7 takes 0.1710 s to operate for a fault at point d, 0.479 s at point b, and 0.8322 s at point a. In the event of a fault at point d, primary relay R7 activates first, whereas, in the event of a malfunction at point b, relay R5 should be activated first. In the event of a failure, the tripping action should be transferred to relay R7.

5.3. Response time of the algorithm

The training of each algorithm (AFDDCNN) using the input training dataset takes about 150 s for all operating scenarios of the ADN. The fault diagnosis algorithm testing, DOST computation, and intelligent protection took 10.123 ms, 4.321 ms, and 20.056 ms, respectively. The intelligent protection technique isolates faults for a different ADN operating mode at an average OT of 34.5 ms, provided that parallel processing is used. The simulation's results complied with the time frame for building a real-time protection strategy with considerable DG penetration.

Table 3. Calculated protection setting and OT for different scenarios of the modified IEEE 13-bus ADN in grid-connected mode with 75% DG penetration.

Fault location	Primary relay	Backup relay	TSM PR1	NPR1	TSM BR1	NBR1	tPR1kl	tBR1kl	CTI
a	R1	R0	0.256	2.543	0.596	2.27	0.33	0.6701	0.3401
b	R2	R1	0.562	5.305	0.213	3.498	0.1238	1.0273	0.9035
b	R3	R1	0.143	3.456	0.438	2.458	0.3692	0.682	0.3128
c	R4	R2	0.129	2.477	0.634	2.157	0.4516	0.8309	0.3793
c	R5	R3	0.123	3.488	0.364	3.118	0.3205	0.6462	0.3257
d	R6	R1	0.697	4.278	0.157	3.514	0.4786	0.8596	0.381
d	R7	R1	0.756	3.191	0.179	2.148	0.5213	0.8637	0.3424
e	R8	R6	0.342	4.187	0.479	2.981	0.498	0.7601	0.2621
e,f	R9	R6	0.245	5.383	0.5447	4.374	0.2369	0.931	0.6941
g	R10	R1	0.921	6.282	0.456	5.546	0.2984	1.0194	0.721
g	R11	R1	0.109	3.991	0.362	3.797	0.5466	0.8465	0.2999
h	R12	R10	0.365	5.715	0.943	4.772	0.4266	1.1966	0.77
h	R13	R11	0.375	4.898	0.496	4.188	0.1762	0.4714	0.2952
i	R14	R12	0.623	3.292	0.849	2.854	0.3364	0.7895	0.4531
i	R15	R13, R17	0.362	3.516	0.355	2.995	0.2546	0.627	0.3724
j	R16	R14	0.2454	2.782	0.492	2.182	0.4695	0.8848	0.4153
j	R17	R4	0.509	2.422	0.141	1.959	0.3291	1.1138	0.7847
k	R18	R12, R15	0.169	8.887	0.055	7.127	0.4823	0.7182	0.2359
k	R19	R13, R14	0.834	4.396	0.027	2.953	0.582	0.8483	0.2663
l	R20	R18	0.219	5.249	0.454	5.434	0.2913	1.1765	0.8852
l	R21	R19	0.169	4.091	0.154	3.112	0.3769	0.9035	0.5266
m	R22	R10, R13, R26	0.774	3.989	0.315	2.684	0.5472	0.8954	0.3482
m	R23	R11, R12, R25	0.056	3.494	0.59	1.924	0.2358	0.8612	0.6254
n	R24	R11, R12, R25	0.519	5.249	0.198	3.768	0.3976	0.7142	0.3166
o	R25	R10, R13, R27	0.171	5.842	0.251	4.896	0.2691	0.6977	0.4286
o	R26	R11, R12, R28	0.863	7.689	0.519	5.247	0.4932	0.863	0.3698
p	R27	R25, R29	0.455	8.254	0.171	6.716	0.3925	0.9268	0.5343
p	R28	R26, R30	0.3678	3.956	0.863	2.384	0.2053	0.6682	0.4629
q	R29	R9, R27	0.943	3.289	0.157	2.946	0.4909	0.9287	0.4378
q,f	R30	R8	0.596	6.681	0.525	5.657	0.2143	0.9005	0.6862
r	R31	R27, R30	0.213	2.549	0.463	2.932	0.4573	0.7538	0.2965

TSM_{PR1}, TSM_{BR1}, N_{PR1}, N_{BR1}, t_{PR1kl}, t_{BR1kl} Time setting, plug setting, and operating time for primary and backup relay in intelligent protection for active 75% penetration of DG in IEEE 13-bus ADN.

6. Comparison with existing protection schemes

The effectiveness of the suggested fault diagnostic scheme and that of several machine learning and deep learning-based fault detection and identification strategies outlined in the literature are compared in Figure 7a [3, 5, 6, 34]. According to the results, the suggested fault diagnosis approach for the ADN was more efficacious than other AI-based methods documented in the literature. The suggested AFDDCNN detects and locates the fault with excellent precision and speed. In addition to fault diagnosis, the intelligent protection scheme is also presented for the test system. The overall OT of primary and backup protection of the protection scheme and of others listed in the literature for the ADN are compared in Figure 7b [12, 16, 17, 35].

The proposed protection scheme has an average minimum primary OT of 0.2633 s and a backup time of 0.4945 s. Table 5 compares the proposed IDOCPS and other protection schemes concerning the number of input cases, fault location, and total OT. It can be seen that the proposed intelligent protection scheme takes a wide variety of cases for training the model, eliminating the miscoordination issues faced in previous works.

The results indicate that the proposed protection scheme's effectiveness for the varying operating conditions with high DG penetration is accurate and faster than other schemes.

Table 4. Calculated protection setting and OT for different scenarios of the modified IEEE 34-bus ADN in grid-connected mode with 40% DG penetration.

Fault location	Primary relay	Backup relay	TSM_{PRI}	N_{PRI}	TSM_{BRI}	N_{BRI}	t_{PRIkl}	t_{BRIkl}	CTI
d	R7	R5, R11	0.247	6.053	0.994	3.946	0.171	0.456	0.285
d	R8	R7, R10	0.517	8.925	0.714	8.391	0.234	0.479	0.245
i	R22	R20, R24	0.958	7.22	0.158	6.349	0.109	0.396	0.287
i	R23	R21, R24	0.369	1.946	0.316	5.681	0.188	0.365	0.177
k	R29	R25, R30, R32	0.763	2.186	0.731	3.605	0.256	0.575	0.319
k	R30	R26, R31,R33	0.174	4.321	0.342	2.137	0.223	0.562	0.339
q	R49	R47, R51, R56	0.969	5.715	0.731	9.445	0.129	0.443	0.314
q	R50	R48, R52, R56	0.765	8.607	0.52	3.273	0.113	0.378	0.265
s	R53	R51, R55	0.286	6.781	0.367	5.72	0.113	0.423	0.31
s	R54	R52, R55	0.853	2.018	0.593	3.504	0.238	0.497	0.259
v	R62	R58, R61, R64	0.342	8.211	0.853	5.712	0.234	0.556	0.322
v	R63	R59, R60, R64	0.158	5.37	0.554	2.948	0.164	0.342	0.178
o	R66	R40, R41, R68	0.354	9.504	0.608	3.695	0.179	0.645	0.466
o	R67	R65, R68	0.343	7.254	0.022	4.322	0.157	0.521	0.364

TSM_{PRI}, TSM_{BRI}, N_{PRI}, N_{BRI}, t_{PRIkl}, t_{BRIkl} Time setting, plug setting, and operating time for primary and backup relay in intelligent protection for active 40% penetration of DG in IEEE 34-bus ADN.

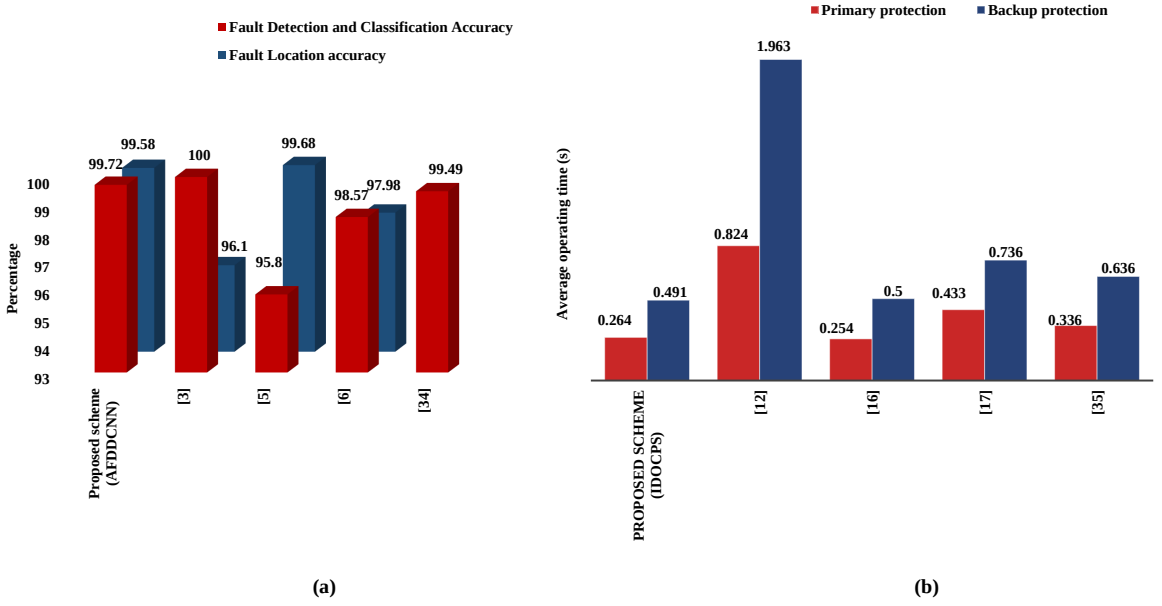

Figure 7. a) Comparative analysis of the proposed scheme with other fault detection algorithms. (b) Performance analysis of the proposed protection scheme with other protection schemes.

Table 5. Comparison of the average response time along with the number of cases considered in the existing protection coordination scheme.

Reference	Fault location	Number of input cases considered	Average response time (s)
[12]	32	314	0.4187
[13]	-	37	31.650
[14]	-	75	0.3891
[16]	10	2564	0.3773
[17]	-	9280	0.4864
[35]	21	42	1.39375
Proposed scheme	200	51158	0.3457

7. Conclusion

With the help of adaptive fault diagnosis using deep learning and DOST, this paper has offered an intelligent protection scheme (IDOCPS) with an MLP-MOFFA-based approach for optimum coordination of the DOCR in ADNs. First, the AFDDCNN model developed in PyTorch was used to train and validate the fault detection/classification and location identification units. Then, using the output of the AFDDCNN, the intelligent protection scheme sent the trip signal to the appropriate section to isolate the faulty part from the ADN. In the IDOCPS, the initial solution of OF was found using MOFFA, and the global optimal solution was determined using the MLP. Thus, the suggested technique combines the benefits of MOFFA and the MLP and eliminates their shortcomings. Both discrete and continuous TSMs and N were achieved using the suggested OF set in current digital relays, greatly minimizing relay OTs and providing acceptable protective coordination between relays. The proposed fault diagnosis algorithm's major benefits are its quick response time (15 ms) and adaptation under different DG penetration scenarios demonstrated on several faults and nonfault transients simulated on the IEEE 13-bus ADN and IEEE 34-bus ADN through EMTP. The simulation results show that the suggested technique produces faster protection of ADNs compared to the conventional method and heuristic algorithm-based methods mentioned in the literature, and its performance is unaffected by changes in system parameters. The significant advantages of this strategy are the trained model's capacity to adapt protection settings to network topology alterations and effectively isolate the fault for a larger DS depending on the parameters obtained during training. The future scope of this work could entail the real-time implementation of the intelligent coordinated protection scheme based on the results obtained from the proposed method and stability analysis for the DS with high DG integration. In addition, the method can be extended to include multiple PMU locations and compared to other deep learning methods.

References

[1] Luo G, Tan Y, Li M, Cheng M, Liu Y et al. Stacked auto-encoder-based fault location in distribution network. IEEE Access 2020; 8: 28043-28053. http://doi.org/10.1109/ACCESS.2020.2971582.

[2] Kandasamy LM, Jaganathan K. Intelligent fault diagnosis using deep learning for a microgrid with high penetration of renewable energy sources. Electric Power Components and Systems 2023; 51 (4): 332-350. http://doi.org/10.1080/15325008.2023.2168091

[3] Chaitanya BK, Yadav A. An intelligent faulty line identification scheme for micro-grids. Iranian Journal of Science and Technology - Transactions of Electrical Engineering 2020; 44 (1): 537-549. http://doi.org/10.1007/s40998-019-00247-x

[4] Gashteroodkhani OA, Majidi M, Etezadi-Amoli M. A combined deep belief network and time-time transform based intelligent protection scheme for microgrids. Electric Power Systems Research 2020; 182: 106239. http://doi.org/10.1016/j.epsr.2020.106239

[5] Liang J, Jing T, Niu H, Wang J. Two-terminal fault location method of distribution network based on adaptive convolution neural network. IEEE Access 2020; 8: 54035-54043. http://doi.org/10.1109/ACCESS.2020.2980573

[6] Jamali S, Bahmanya A, Ranjbar S. Hybrid classifier for fault location in active distribution networks. Protection and Control of Modern Power Systems 2020: 5 (1): 17. http://doi.org/10.1186/s41601-020-00162-y

[7] Rai P, Londhe ND, Raj R. Fault classification in power system distribution network integrated with distributed generators using CNN. Electric Power Systems Research 2021; 192: 106914. https://doi.org/10.1016/j.epsr.2020.106914

[8] Gush T, Bukhari SBA, Mehmood KK, Admasie S, Kim JS et al. Intelligent fault classification and location identification method for microgrids using discrete orthonormal stockwell transform-based optimized multi-kernel extreme learning machine. Energies (Basel) 2019; 12 (23): 4504. http://doi.org/10.3390/en12234504

[9] Reddy MJB, Gopakumar P, Mohanta DK. A novel transmission line protection using DOST and SVM. Engineering Science and Technology, an International Journal 2016; 19 (2): 1027-1039. http://doi.org/10.1016/j.jestch.2015.12.011

[10] Kumar DS, Srinivasan D, Reindl T. A fast and scalable protection scheme for distribution networks with distributed generation. IEEE Transactions on Power Delivery 2016; 31 (1): 67-75. http://doi.org/10.1109/TPWRD.2015.2464107

[11] Kar S, Samantaray SR. A fuzzy rule base approach for intelligent protection of microgrids. Electric Power Components and Systems 2015; 43: 2082-2093. http://doi.org/10.1080/15325008.2015.1070384

[12] Baghaee HR, Mirsalim M, Gharehpetian GB, Talebi HA. MOPSO/FDMT-based Pareto-optimal solution for coordination of overcurrent relays in interconnected networks and multi-DER microgrids. IET Generation, Transmission and Distribution 2018; 12 (12): 2871-2886. http://doi.org/10.1049/iet-gtd.2018.0079

[13] Korashy A, Kamel S, Nasrat L, Jurado F. Developed multi-objective grey wolf optimizer with fuzzy logic decision making tool for direction overcurrent relays coordination. Soft Computing 2020; 24 (17): 13305-13317. http://doi.org/10.1007/s00500-020-04745-7

[14] Alkaran DS, Vatani MR, Sanjari MJ, Gharehpetian GB, Naderi MS. Optimal overcurrent relay coordination in interconnected networks by using fuzzy-based GA method. IEEE Transactions on Smart Grid 2018; 9 (4): 3091-3101. http://doi.org/10.1109/TSG.2016.2626393

[15] Moravej Z, Ooreh OS. Coordination of distance and directional overcurrent relays using a new algorithm: grey wolf optimizer. Turkish Journal of Electrical Engineering and Computer Sciences 2018; 26 (6): 3130-3144. http://doi.org/10.3906/elk-1803-123

[16] Dawoud MA, Ibrahim DK, Gilany MI, El'gharably A. Proposed application for rate of change of phasor voltage in fault detection and coordination studies in MV distribution networks. Iranian Journal of Science and Technology - Transactions of Electrical Engineering 2021; 45 (3): 815-831. http://doi.org/10.1007/s40998-020-00402-9

[17] Sadoughi M, Hojjat 1M, Abardeh MH. Smart overcurrent relay for operating in islanded and grid-connected modes of a micro-grid without needing communication systems. Energy Systems 2022; 13 (1): 31-51. http://doi.org/10.1007/s12667-020-00381-0

[18] Usman MU, Faruque MO. Validation of a PMU-based fault location identification method for smart distribution network with photovoltaics using real-time data. IET Generation, Transmission and Distribution 2018; 12 (21): 5824-5833. http://doi.org/10.1049/iet-gtd.2018.6245

[19] Liu J, Tang J, Ponci F, Monti A, Muscas C et al. Trade-offs in PMU deployment for state estimation in active distribution grids. IEEE Transactions on Smart Grid 2012; 3 (2): 915-924. http://doi.org/10.1109/TSG.2012.2191578

[20] Kersting WH. Radial distribution test feeders. IEEE Transactions on Power Systems 1991; 6 (3): 975-985. http://doi.org/10.1109/59.119237

[21] Ghaderi A, Mohammadpour HA, Ginn HL, Shin YJ. High-impedance fault detection in the distribution network using the time-frequency-based algorithm. IEEE Transactions on Power Delivery 2015; 30 (3): 1260-1268. http://doi.org/10.1109/TPWRD.2014.2361207

[22] Stockwell RG. A basis for efficient representation of the S-transform. Digital Signal Processing: A Review Journal 2007; 17 (1): 371-393. http://doi.org/10.1016/j.dsp.2006.04.006

[23] Battisti U, Riba L. Window-dependent bases for efficient representations of the Stockwell transform. Applied and Computational Harmonic Analysis 2016; 40 (2): 292-320. http://doi.org/10.1016/j.acha.2015.02.002

[24] Reddy MJB, Raghupathy RK, Venkatesh KP, Mohanta DK. Power quality analysis using discrete orthogonal S-transform (DOST). Digital Signal Processing: A Review Journal 2013; 23 (2): 616-626. http://doi.org/10.1016/j.dsp.2012.09.013

[25] Schmidhuber J. Deep learning in neural networks: an overview. Neural Networks 2015; 61: 85-117. http://doi.org/10.1016/j.neunet.2014.09.003

[26] Cho H, Kim Y, Lee E, Choi D, Lee Y et al. Basic enhancement strategies when using Bayesian optimization for hyperparameter tuning of deep neural networks. IEEE Access 2020; 8: 52588-52608. http://doi.org/10.1109/ACCESS.2020.2981072

[27] Mitchell TM. Machine Learning. New York, NY, USA: McGraw Hill, 1997.

[28] Gers JM, Holmes EJ. Protection of Electricity Distribution Networks. Stevenage, UK: IET, 2011. http://doi.org/10.1049/PBPO065E

[29] Meshram SG, Meshram C, Pourhosseini FA, Hasan MA, Islam S. A multi-layer perceptron (MLP)-fire fly algorithm (FFA)-based model for sediment prediction. Soft Computing 2019; 26 (2): 911-920. https://doi.org/10.1007/s00500-021-06281-4

[30] Yang XS. Nature-Inspired Optimization Algorithms. Dordrecht, the Netherlands: Elsevier, 2014. http://doi.org/10.1016/C2013-0-01368-0

[31] Ghorbani MA, Shamshirband S, Haghi D, Azani A, Bonakdari H et al. Application of firefly algorithm-based support vector machines for prediction of field capacity and permanent wilting point. Soil Tillage Research 2017; 172: 32-38. http://doi.org/10.1016/j.still.2017.04.009

[32] Khurshaid T,Wadood A, Farkoush S, Kim CH, Yu J et al. Improved firefly algorithm for the optimal coordination of directional overcurrent relays. IEEE Access 2019; 7: 78503-78514. http://doi.org/10.1109/ACCESS.2019.2922426

[33] Zarei SF, Parniani M. A comprehensive digital protection scheme for low-voltage microgrids with inverter-based and conventional distributed generations. IEEE Transactions on Power Delivery 2017; 32 (1): 441-452. http://doi.org/10.1109/TPWRD.2016.2566264

[34] Guo MF, Zeng XD, Chen DY, Yang NC. Deep-learning-based earth fault detection using continuous wavelet transform and convolutional neural network in resonant grounding distribution systems. IEEE Sensors Journal 2018; 18: 1291-1300. http://doi.org/10.1109/JSEN.2017.2776238

[35] Khandare P, Deokar SA, Dixit AM. Optimization techniques using DWT-differentiation algorithms for fault detection and relay coordination in microgrid. Electrical Engineering 2021; 103 (1): 493–503. http://doi.org/10.1007/s00202-020-01089-1